THE AMERICAN SOCIETY OF MECHANICAL ENGINEERS
345 E. 47 St., New York, N.Y. 10017

82-GT-267

Modal Balancing of a Multi-Mass Flexible Rotor Without Trial Weights

A. B. Palazzolo
Assistant Professor,
Department of Mechanical and Aerospace Engineering

E. J. Gunter
Professor,
Department of Mechanical and Aerospace Engineering
Director,
Rotor Dynamics Laboratory
Mem. ASME

University of Virginia,
Charlottesville, VA

In this paper, a procedure is presented to determine the unbalance distribution in a multi-mass flexible rotor system without requiring that trial weights be placed upon the shaft to first determine the influence coefficient matrix of the various balance planes. A modified Nyquist plotting procedure is presented to generate a polar plot of proximity probe measurements for determination of the 90-deg phase shift position of the modal eccentricity. By knowing the rotor modal mass and mode shape, a modal balancing distribution can be calculated. This relationship provides a quick procedure in estimating a first mode balance correction weight in both magnitude and angular location. An application is presented for a steam turbine during the startup of a hydrogen gas compression train. Higher order modal unbalance corrections are shown to be calculable in a similar manner.

NOMENCLATURE

A_i frequency dependent amplification factor for ith mode

A_c amplification factor at undamped critical speed

A_u amplification factor at unbalance resonance speed

$\bar{A}$ normalized amplification factor

[C] system damping matrix

C_r damping constant associated with r_{th} mode

C_{rs} cross coupled modal damping coefficient

E_i modal eccentricity of ith mode

$e^{i\omega t}$ periodic reference factor = $\cos\omega t + i \sin\omega t$

f_1 ratio of rotor speed to rotor first critical speed $f_1 = N/N_1 = \omega/\omega_1$

f_r ratio of rotor speed to rth rotor critical speed $f_r = N/N_r = \omega/\omega_r$

i imaginary number prefix

j degree of freedom index

[K] system stiffness matrix

K_r modal stiffness of r_{th} mode

[M] system mass and rotational inertia matrix

M_1 modal mass of first mode

M_r modal mass of r_{th} mode

n number of degrees of freedom of system

N shaft rotational speed in RPM

N_1 shaft first critical speed in RPM

N_r shaft r_{th} critical speed in RPM

{Q} vector of complex displacement coefficients which describe the periodic response of the system

q_j complex displacement coefficient for jth degree of freedom

q_j magnitude of q_j

ϕ_j phase angle of q_j referenced with respect to the alignment of a shaft notch with a stationary detector

{q} vector of time dependent elements which describes the system's displacements

r index for mode number

s index for mode number

{U} vector of complex force coefficients, i.e. magnitude and phase. The phase angle is again referenced with respect to the alignment of a shaft notch with a stationary detector.

Contributed by the Gas Turbine Division of the ASME.

U_j complex shaft unbalance acting along the line of the jth degree of freedom

$\bar{U}_1$ modal unbalance of first mode $\bar{U}_1 = (\Lambda_1 + i\mu_1)$

U_{c1} correction imbalance applied to the rotor balance plane

$\Lambda_1 + i\mu_1$ first modal unbalance eccentricity in rectangular form.

Note $\Lambda_1 + i\mu_1 = \bar{U}_1 = \bar{E}_1 e^{i\phi_u}$

$\Lambda_r + i\mu_r$ rth modal unbalance eccentricity

ξ_1 first modal damping factor

ξ_r rth modal damping factor

ξ_{rs} cross coupled modal damping factor

ψ_{ij} component of the ith mode shape at jth degree of freedom (or probe location)

$\{\psi^r\}$ rth mode shape

ϕ_u modal unbalance angle referenced to the probe direction. Positive in the direction of shaft rotation.

ϕ_{c1} angle of the correction imbalance referenced to the probe direction. Positive in the direction of rotation.

γ_s sth mode shape coefficient

ω shaft rotational speed in radians/second

ω_i shaft ith critical speed in radians/second

I. INTRODUCTION

In the chemical process and related industries, many steam or gas turbines and multi-stage centrifugal compressors have normal operating speeds between their first and second rotor critical speeds. It is a wise procedure to minimize the shaft vibratory response, measured at the bearings, while traversing through the first critical. This practice should guarantee low vibrations levels in the operating speed range and the avoidance of internal seal rubs. If an influence coefficient balancing method is employed to reduce these vibrations, an initial trial weight must be placed on the rotor. The magnitude and location of this weight is so critical that it will in some cases decide the success or failure of the balance attempt. The analysis and application of a balancing technique is presented here, which predicts a proper trial weight and that should reduce the critical speed vibration amplitudes considerably.

Similar previous work was done by the authors Bishop, Parkinson, Jackson and Lindley (1,2,3,4,5), and by Kellenberger (6), Lindsey (7), and LeGrow (8). Though this literature is closely related, the technique presented in this paper eliminates the prior assumption of coincidence between the unbalance response peak and the critical speed. This provides a more accurate estimate of the effective modal unbalance and modal damping factor.

The method assumes the predominance of a specific mode in the vicinity of its associated frequency range. This assumption isolates the mode and provides a basis for analytically relating the response measurements to the unknown mass unbalances along the rotor. The analysis requires knowledge of the shaft mode shape of interest and the associated modal mass. These quantities may be estimated from a critical speed computer program model.

The actual vibration measurements utilized should be of shaft absolute motion, i.e. relative to space. This would typically be attained with the instantaneous electronic addition of shaft relative to bearing housing and bearing housing relative to space transducer signals. Due to high casing to shaft weight ratios, many machines exhibit very low casing vibration response levels compared to shaft response levels. In these instances, shaft motion relative to the bearing housing will closely approximate shaft absolute motion (9).

Measurements must be conditioned to represent only the portion of the response attributable to unbalance. This is accomplished by directing the transducer signals through a digital vector or tracking filter. This instrument narrow bandpass filters the raw data, with center frequency at the shaft rotational speed. This final conditioned "synchronous" signal is depicted in Figure 1 along with the response phase angle convention used in the analysis.

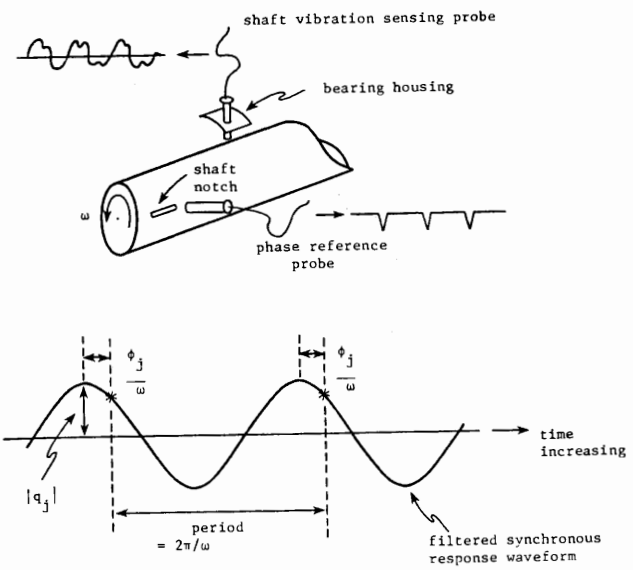

Fig. 1. Illustration of phase angel convention used in the analysis and actual measurement.

II. ROTOR DYNAMICAL EQUATIONS OF MOTION

The generalized equations of motion for a rotor bearing system may be expressed in the matrix form as follows (see Appendix A)

$$[M]\{\ddot{q}\} + [C]\{\dot{q}\} + [K]\{q\} = \omega^2 U e^{i\omega t} \quad (2.1)$$

The generalized displacement vector $\{q\}$ is composed of both displacements and rotations in the XZ and YZ planes respectively. The mass matrix [M] contains both the mass terms and the transverse moments of inertia for the N stations considered. For a general multi-stage turborotor, the number of degrees of freedom in the system can be quite large. The order of the system, however may be considerably reduced by expressing the displacement field $\{q\}$ in terms of a finite number of planar mode shapes corresponding to the undamped system such that

$$\{q\} = \gamma_1\{\psi_1\} + \gamma_2\{\psi_2\} + \gamma_3\{\psi_3\} \ . \ . \ . \quad (2.2)$$

For the case of a turborotor which has two resonance frequencies in the operating range, the use of the first four modes in the modal expansion is usually sufficient.

Upon application of orthogonality, the modal equations of motion are of the form

$$\ddot{\gamma}_r + 2 \sum_{s=1}^{n} \xi_{rs} \omega_s \dot{\gamma}_s + \omega_r^2 \gamma_r = \omega^2 E_r e^{i\omega t} \quad (2.3)$$

Appendix A shows that, in general, the use of the undamped planar modes will not completely uncouple the modal equations of motion. The effect of the modal cross coupling damping coefficients ξ_{rs} is to couple the planar modes of motion in a system with discrete bearing damping locations to form a complex rotor mode shape that is skewed or nonplanar. This space skew effect is more pronounced near the bearings.

The motion of a turborotor operating through two critical speeds may be represented approximately in terms of its first three planar modes as follows

$$\{q\} = \gamma_1[\{\psi_1\} - i2\ \xi_{31}\ f_3\ \{\psi_3\}] + \gamma_2\ \{\psi_2\} \quad (2.4)$$

Assume that if the rotor speed is in the vicinity of the first critical, the first mode predominates the response. Then equation (2.4) implies for motion near the rotor center span

$$q_j = \frac{(\Lambda_1 + i\mu_1)\ f_1^2\ \psi_{1j}}{(1 - f_1^2 + i2\xi_1 f_1)} = E_1 A_1 \psi_{1j} \quad (2.5)$$

In the above equation the rotor modal mass may be calculated, along with the rotor mode shapes, from a standard critical speed code. The modal mass is given by

$$m_1 = \int_o^L \rho(x)\ \psi_1^2\ dx = \sum_{j=1}^{N} w_j\ \psi_{1j}^2/g \quad (2.6)$$

The rotor modal mass for the first mode for a multistage compressor normally lies between 55 to 65% of the total rotor mass.

The problem of modal balancing of a system that behaves in a fashion similar to Equation (2.5) reduces to the determination of the complex modal eccentricity value E_1. The modal unbalance U_1 is given be

$$U_1 = m_1\ E_1 = \Lambda_1 + i\mu_1 \quad (2.7)$$

More than one balancing plane may be used to achieve the required modal balancing value U_1. In the case of three balancing planes the modal unbalance value U_1 is equivalent to

$$U_1 = U_1\ \psi_{11} + U_2\ \psi_{12} + U_3\ \psi_{13} \quad (2.8)$$

In order to accurately determine the modal unbalance eccentricity E_1 without the use of trial weights, we must be able to determine from an examination of the experimental data, the principal modal damping coefficient ξ_{rr}. There are several ways to achieve this. One may use the half power point procedure in which the rotor speeds are determined corresponding to the speeds where the amplitude of motion is equal to $1/\sqrt{2}$ times the resonance frequency amplitude. The damping in the system is then given by

$$\xi = \frac{N_2 - N_1}{N_2 + N_1} \quad (2.9)$$

The amplification factor at the undamped critical speed is given by

$$A_c = \frac{1}{2\xi} \quad (2.10)$$

At this frequency, the modal eccentricity vector E_i is leading the modal coordinate γ_i by 90°. By properly identifying the speed and phase angle at which the 90° shift occurs, the location of the plane for modal balancing may be determined. It should be noted that the maximum amplitude of motion does not occur at the undamped critical speed. The maximum amplitude occurs at a speed of

$$N_u = \frac{N_c}{\sqrt{1 - 2\xi^2}} \quad (2.11)$$

The amplification factors A_u at the maximum response speed is given by

$$A_u = \frac{A_c}{\sqrt{1 - \xi^2}} \quad (2.12)$$

The relative displacement eccentricity phase angle at this speed is always larger than 90°. The problem then of modal balancing without resorting to the application of an initial trial weight, then becomes a problem in accurately determining the damping ratio ξ for the mode and the speed at which the 90° modal eccentricity phase shift occurs. These two values may be determined by means of a modified Nyquist or polar plotting procedure as described in the following sections.

Figure 2 represents the amplitude and phase angle motion of an experimental 3 mass rotor system with the measurement point near the center span.

Table 1 is a computer simulation of the experimental Centritech rotor at the University of Virginia Rotor Dynamics Laboratory, with 4.3 gm-in located at the zero ref. position. The undamped critical speed is predicted to be at 2484 RPM. Note that at this speed, the phase angle is lagging the timing reference mark by 90°. However, Table 1 clearly shows that the maximum rotor amplitude does

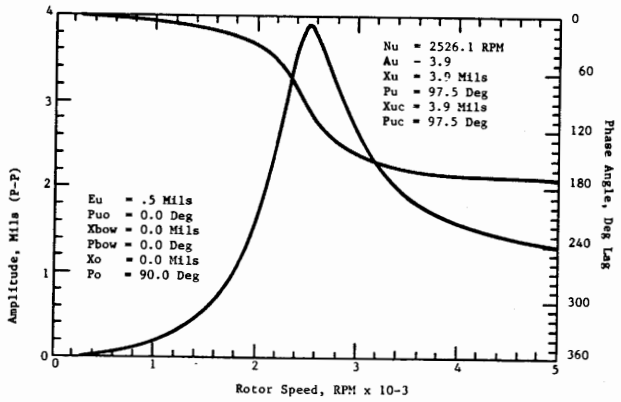

Fig. 2. Simulation of 3-mass Centritech Rotor X-2 midspan location -1st mode.

not occur at the undamped critical speed but at the slightly higher speed of 2526 RPM. At this speed, the phase angle lag is 97.5°. Figure 2 shows the corresponding rotor amplitude and phase plotted. If one were to assume that the mass center (or modal mass center E_1 in this case) is leading the maximum response amplitude by 90°, then there would be an error of 7.5% on the angular estimation of the unbalance location. The speed at which the 90° phase shift occurs can be determined by means of a modified Nyquist or polar plot.

Table 1

Simulation of Experimental Centritech Rotor with First Mode Excitation

x-2 Midspan Location -1 st Mode

Weight LB	Stiffness LB/IN	Damping LB-SEC/IN
19	3330	3.3

ZETA(DIM)	Cc(LB-SEC/IN)	Acr(DIM)	Amax(DIM)
.129	25.606	3.880	3.912

Ncr(RPM) (Undamped Critical)	Nd (Damped Critical)	Nu (Resonance Speed)
2484	2463	2526

MASS UNBALANCE = 4.3 GM-IN

SIMULATION OF 3-MASS CENTRITECH ROTOR
x-2 MIDSPAN LOCATION -1 st MODE CASE NO. 1.0

RPM	x (UNCORRECTED) (P-P MILS)	XC (MILS)	PHASE (UNCORRECTED) (Deg)	PHASEC (Deg)	AMP FACTOR (DIM)
25 2400	3.62	3.62	75.09	75.09	3.55
26 2484	3.88	3.88	90.00	90.00	3.86 N_{cr}
27 2500	3.90	3.90	92.89	92.89	3.86
28 2526	3.91	3.91	97.47	97.47	3.80 N_u
29 2600	3.83	3.83	109.55	109.55	3.42
30 2800	3.20	3.20	132.99	132.99	2.22

III. MODIFIED NYQUIST PLOT

Equation (2.5) shows that the complex rotor amplitude {q} at the jth location is a function of the modal unbalance eccentricity E_i, the modal displacement ψ_{ij} corresponding to the jth location, and a complex amplification factor A_i. Where

$$A_i = \frac{f_i^2}{1 - f_i^2 + i2\,\xi_i f_i} = R_i e^{-i\phi_i} \qquad (3.1)$$

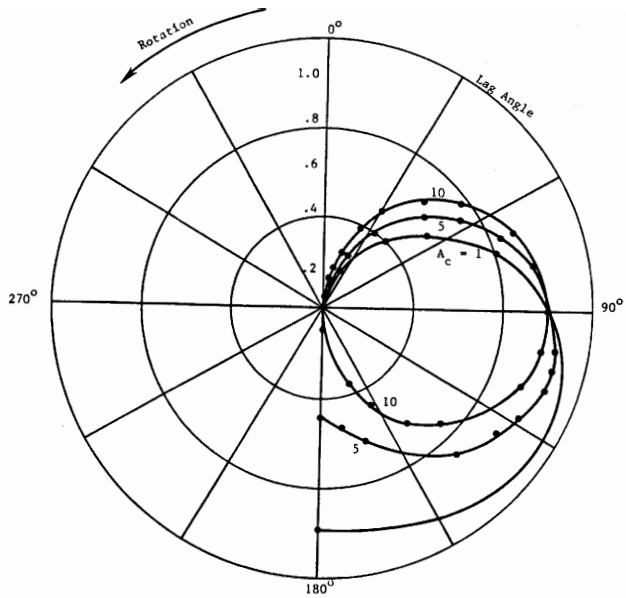

Fig. 3. Polar plot of relative amplification factor $\bar{A}$ for various values of A_c.

where

$$R = \frac{f^2}{\sqrt{(1 - f^2)^2 + (2\xi f)^2}}$$

$$\tan \phi = \frac{2\xi f}{1 - f^2}$$

When f = 1, the frequency ratio corresponds to the undamped critical speed. The amplification factor at the undamped critical speed is

$$A_c = \frac{1}{i2\xi} = -\frac{i}{2\xi} \qquad (3.2)$$

Fig. 3 represents a plot of the relative amplification function

$$\bar{A} = 2\xi\, A \qquad (3.3)$$

At the critical speed (f=1) the value of $\bar{A}$ is 1 for all values of damping and the phase lag is 90°. Fig. 3 represents a polar plot of the relative amplification factor $\bar{A}$ for various values of A_c (1,5,10). For very high values of A_c (or lightly damped systems) the plot will approach a unit circle. For moderate to heavy values of damping, as given by the values of A_c = 5 and 1, the maximum amplitude does not occur at the 90° phase lag position and the curve becomes considerably distorted from a circle. It will be shown that the function $\bar{A}$ can be transformed into a unit circle by the following procedure. Consider the complex quantity:

$$\frac{f}{(1 - f^2 + i\ 2\ \xi f)}$$

Separating this into real and imaginary parts, i.e. (x + iy);

$$x = \frac{f(1 - f^2)}{(1 - f^2)^2 + (2\xi f)^2}$$

$$y = \frac{- 2\xi f^2}{(1 - f^2)^2 + (2\xi f)^2}$$

It follows:

$$x^2 + (y + \frac{1}{4\xi})^2 = \qquad (3.4)$$

$$\frac{\{(1 - f^2)^4 + (1 - f^2)^2 (8\xi^2 f^2) + 16\xi^4 f^4\}}{16\xi^2 \{(1 - f^2)^4 + 8\xi^2 f^2 (1 - f^2)^2 + 16\xi^4 f^4\}} = \frac{1}{16 \xi^2}$$

This is the locus of a circle in the complex plane with:

center: $(0, - \frac{1}{4\xi})$ and diameter: $\frac{1}{2\xi}$

Therefore it is seen from Equation (3.4) that the ratio of the speed dependent amplification function divided by the frequency ratio f plots into a circle with the maximum amplitude = $A_c = 1/2\xi$.

This circle is represented in Figure 4 by the dashed line. Note that the position on this circle corresponding to the critical speed ($N = N_1$) can easily be found by setting $f_1 = 1$ in equation (3.4). The coordinates of this point are then $(0, - 1/(2\xi_1))$. This point is at the bottom of the circle on the negative imaginary axis. Then the critical speed occurs at exactly one diameter from the origin. Rearranging equation (2.5) shows

$$\left(\frac{q_j}{f_1 \psi_{1j}}\right) =$$

$$\text{sgn } \{\psi_{1j}\} \ (\Lambda_1 + i\mu_1) \quad \frac{f_1}{(1 - f_1^2 + i\ 2\xi_1 f_1)} \qquad (3.5)$$

where $\text{sgn } \{\psi_{1j}\} = 1, \quad \psi_{1j} > 0$

$\qquad\qquad\qquad - 1, \quad \psi_{1j} < 0$

In this form the modal unbalance eccentricity $(\Lambda_1 + i\mu_1)$ rotates the circle counterclockwise through the angle;

$$\phi_u = \tan^{-1} (\mu_1/\Lambda_1)$$

and changes its diameter to

$$\frac{\sqrt{\Lambda_1^2 + \mu_1^2}}{2\xi_1} = \frac{E_1}{2\xi_1}$$

The analytical expression for the quantity to be measured is obtained from equation (3.5) as:

$$\frac{q_j}{N} = \qquad (3.6)$$

$$\left(\frac{\psi_{1j}}{N_1}\right) \ E_1 \ \text{sgn } \{\psi_{1j}\} \ e^{i\phi_u} \ \frac{f_1}{(1 - f1^2 + i\ 2\xi_1 f_1)}$$

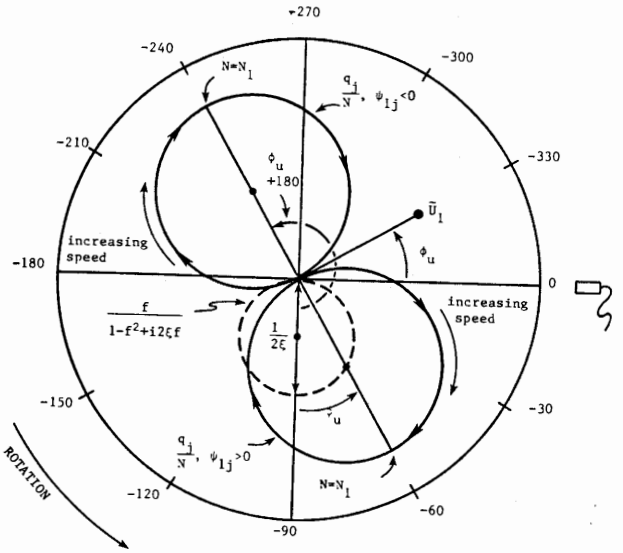

Fig. 4. Modified polar response plot. Zero degrees is transducer direction when notch and kϕ aligned.

The expression for the circle diameter in Figure 4 is now

$$\frac{\psi_{1j} \cdot \bar{U}_1}{2 \cdot m_1 \cdot N_1 \cdot \xi_1} \qquad (3.7)$$

From the preceding discussion, the critical speed occurs at one diameter from the origin in equation (3.6). Therefore, the diameter may also be expressed

$$\frac{q_j \Big|_{N = N_1}}{N_1} \qquad (3.8)$$

Equations (3.7) and (3.8) then imply

$$\bar{U}_1 = \frac{2 \cdot m_1 \cdot \xi_1 \ q_j \Big|_{N = N_1}}{\psi_{1j}} \qquad (3.9)$$

Equation (3.9) is an expression for the magnitude of the shaft first modal unbalance; however the damping factor (ξ_1) is still unknown. This may be calculated by considering the phase angle of the response as measured at the probe location. Consider the response equation (2.5) in polar form

$$q_j = \frac{\bar{U}_1 \cdot \psi_{1j}}{m_1} \cdot \frac{f_1^2}{\sqrt{(1 - f_1^2)^2 + (2\xi_1 f_1)^2}}$$

= amplitude of measured synchronous response (3.10)

$$\phi_j = \phi_u + \tan^{-1} \left\{\frac{- 2\xi_1 f_1}{1 - f_1^2}\right\} \qquad (3.11)$$

= phase angle of measured synchronous response (radians)

Taking the frequency derivative of the response phase angle shows

$$\frac{d}{d\omega}(\phi_j) = \frac{d}{d\omega}\left(\tan^{-1}\left\{\frac{-2\xi_1 \omega\omega_1}{\omega_1^2 - \omega^2}\right\}\right)$$

$$= \frac{(\omega_1^2 - \omega^2)(-2\xi_1\omega_1) + (2\xi_1\omega\omega_1)(-2\omega)}{(\omega_1^2 - \omega^2)^2 + (-2\xi_1\omega\omega_1)^2}$$

Evaluating this expression at the critical speed shows

$$\left.\frac{d}{d\omega}(\phi_j)\right|_{\omega=\omega_1} = \frac{-1}{\omega_1\xi_1} \qquad (3.12)$$

Expressing this relationship in revolutions per minute (RPM) and degrees

$$\frac{1}{2\xi_1} = \frac{N_1\pi}{360} \cdot \left(\frac{-\Delta\phi_j}{\Delta N}\bigg|_{N=N_1}\right) = Ac_1 \qquad (3.13)$$

where

$$\left.\frac{\Delta\phi_j}{\Delta N}\right|_{N=N_1}$$

is the slope of the phase angle versus shaft speed curve at the first critical speed in degrees per RPM.

Substituting equation (3.13) into equation (3.9) provides an expression for the modal unbalance magnitude in terms of measured or calculable quantities

$$\bar{U}_1 \cdot g \qquad (3.14)$$

$$= \frac{360 \cdot (m_1 \cdot g)}{\pi \cdot \psi_{1j}} \cdot \left\{\frac{\frac{q_j}{N}}{\frac{-\Delta\phi_j}{\Delta N}}\right\}\Bigg|_{N=N_1} \cdot \text{degrees}$$

g = gravitation constant = 386 in/s^2

m_1 = first modal mass in lb · s^2 · in^{-1}

ψ_{1j} = shaft first mode shape component at probe location, dimensionless

q_j = amplitude of shaft synchronous response at the probe location, inches (mils/1000)

ϕ_j = phase angle of shaft synchronous response at the probe location, degrees

The modal unbalance, $\bar{U}_1$, can now be determined in magnitude (Equation 3.14) and phase angle (Figure 4) with shaft vibration measurements recorded through the critical speed range.

The modal unbalance can be nulled by the addition of a proper correction weight to a balance plane of the shaft. To calculate the correction weight, consider the definition of the modal unbalance from equation (A.13b) of Appendix A.

$$\bar{U}_1 = \Lambda_1 + i\mu_1$$

$$= \psi_{11}U_1 + \psi_{12}U_2 + \cdots \psi_{1b}U_b + \cdots \psi_{1n}U_n$$

where ψ_{1b} is the first mode shape component at the balance plane location. With the addition of a correction mass, U_{c1}, to the balance plane the modal unbalance becomes

$$\bar{U}_{1\ \text{after}} = \psi_{11}U_1 + \psi_{12}U_2 + \ldots\psi_{1b}(U_b + U_{c1}) + \ldots\psi_{1n}U_n$$

$$= \bar{U}_1 + \psi_{1b}U_{c1}$$

Requiring that the final modal unbalance becomes zero produces the correction weight equation

$$U_{c1} = -\bar{U}_1/\psi_{1b} \qquad (3.15)$$

IV. APPLICATION ON INDUSTRIAL STEAM TURBINE

The use of the preceding theory is illustrated with the vibration response of a steam turbine driver in a hydrogen compression train. In this case, it was requested by plant personnel to estimate the amount of unbalance in the turbine rotor.

Figure 5 is an unbalance response plot of synchronous response amplitude and phase angle made during the train startup. The transducer used was a shaft relative displacement-proximity probe, permanently installed in the turbine inlet end bearing housing. This data has been electronically compensated for false slow roll data, induced by shaft surface imperfections and magnetic inhomogeniety. Note that the amplitude scale is labeled in units of mils peak to peak divided by 2, since the readout of the instrument used for the measurement is in mils peak to peak. Additionally, the phase angle scale is in negative degrees since the measurement instrument readout is 360° minus ϕ_j (see Figure 1).

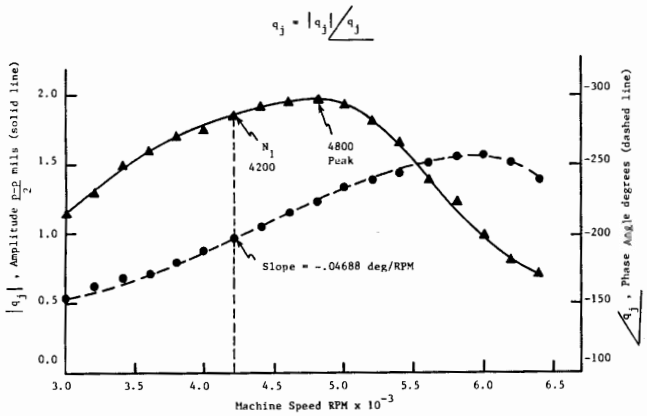

Fig. 5. Shaft unbalance response plot at turbine inlet end bearing.

Table 2 lists the data from Figure 5 required in using the theoretical development. This table is divided into three columns: rotor speeds, transducer synchronous response reading, and the same reading divided by the rotor speed. The second column quantities correspond with equations (3.10) and (3.11), while the third column corresponds to equation (3.6) and the polar plot in Figure 6. Figure 6 is a polar plot of the numbers in column 3. Comparison of this figures with Figure 4 identifies the critical speed to be 4200 RPM. This speed does

not correspond to the peak response speed (4800 RPM) shown in Figure 5. The graphical isolation of the critical speed from the unbalance response peak provides for a more accurate evaluation of Eq. (3.14). Also, comparing Figures 4 and 6 identifies the modal unbalance angle to be $\phi_u = 252°$, since $\psi_{1j} > 0$ as shown in Figure 7.

Table 2

Turbine Response Data from Fig. 5 and the Polar Plot Parameter q_j/N

N	q_j, ϕ_j	q_j/N
RPM	mils, degrees	(mils/RPM)x10^{-4}
3000	1.15, - 154	3.833, - 153
3200	1.30, - 162	4.063, - 162
3400	1.50, - 168	4.412, - 168
3600	1.60, - 172	4.444, - 172
3800	1.70, - 180	4.474, - 180
4000	1.75, - 189	4.375, - 189
4200	1.85, - 198	4.405, - 198
4400	1.93, - 205	4.390, - 205
4600	1.95, - 216	4.241, - 216
4800	1.98, - 224	4.125, - 224
5000	1.95, - 234	3.900, - 234
5200	1.85, - 240	3.560, - 240
5400	1.65, - 245	3.056, - 245
5600	1.40, - 252	2.500, - 252
5800	1.25, - 256	2.155, - 256
6000	1.00, - 258	1.666, - 258
6200	0.83, - 252	1.340, - 252
6400	0.73, - 240	1.141, - 240

The mode shape shown in Figure 7 was generated from a 10 mass station computer model of the turbine rotor. This same model calculates the first modal weight to be 455 lbs. The magnitude of the first modal unbalance may now be calculated from equation (3.14),

$$\bar{U}_1 \cdot g = \frac{360 \cdot (m_1 \cdot g)}{\pi \cdot \psi_{1j}} \cdot \left\{ \frac{\frac{q_j}{N}}{\frac{-\Delta\phi_j}{\Delta N}} \right\}_{N=N_1} \cdot \text{degrees}$$

$$= \frac{360 \cdot (455 \text{ lbs})}{\pi \cdot (0.7607)} \cdot \left\{ \frac{4.405 \times 10^{-7} \text{ in./RPM}}{0.04688°/\text{RPM}} \right\} \cdot \text{degrees}$$

$$= 0.644 \text{ lb.in.} = 10.3 \text{ oz.in.}$$

where the quantities are obtained from

ψ_{1j}: Figure 7

$\left.\frac{q_j}{N}\right|_{N=N_1}$: Table 2

$\left.\frac{\Delta\phi_j}{\Delta N}\right|_{N=N_1}$: Figure 5

The modal unbalance weight can now be expressed as

$$\bar{U}_1 = 10.3, \quad 252° \text{ oz.in.}$$

The correction weight to be applied at the balance plane is calculated from equation (3.15):

$$U_{c1} = - \bar{U}_1/\psi_{1b}$$

where ψ_{1b} is approximately 0.80 from Figure 7. Therefore

$$U_{c1} = (- 10.3, 252°)/0.80 \text{ oz.in.}$$

$$= (12.9, \quad 72°) \text{ oz.in.}$$

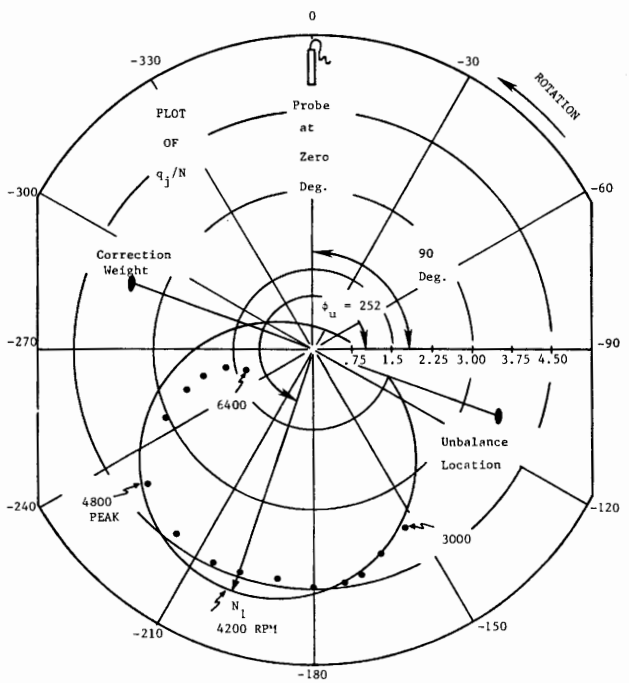

Fig. 6. Polar plot of turbine unbalance response vectors divided by rotational speed, in units of mils/RPM x 10^{-4}.

Since this is a rather large balance correction weight for this size of rotor, a safety reduction factor of between 2 and 3 should be applied to its magnitude before actual attachment. The reason for this high magnitude can easily be seen from the response curves shown in Figure 5. Unsually high damping is present in this rotor-bearing system as is implicated by the broad amplitude response and small phase angle slope. Actual attachment of the correction weight is illustrated in Figure 8.

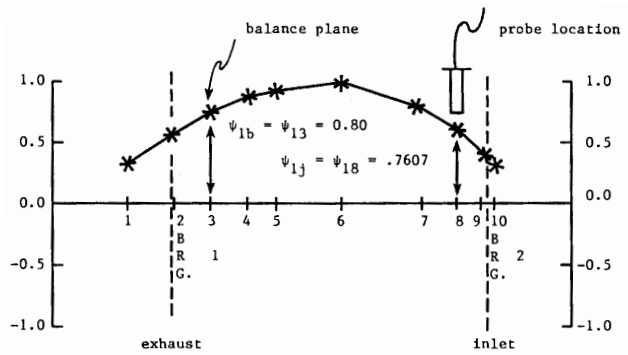

Fig. 7. Turbine rotor - first mode shape. Note the balance plane and probe location modal components.

V. BALANCING OF HIGHER MODES AND THEORETICAL LIMITATIONS

Examining the equations of the theoretical analysis section reveals that the same procedure may be followed in calculating higher order modal unbalances. This is most easily seen by simply changing subscripts in (3.1).

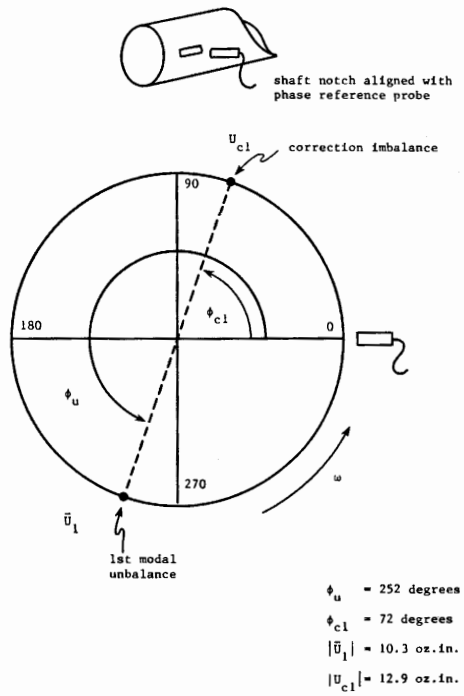

Fig. 8. Location of the first modal unbalance and the correction imbalance on the steam turbine balance plane.

To effectively balance several modes, the corresponding modal unbalances must be simultaneously nulled. This requires that the number of balance planes used must equal the number of modes considered. This condition leads to the development of a system of simultaneous equations to be solved for the correction weights. These are derived in the same manner as Equation (3.15).

Considering the 2 mode case, the requirements for nulling the first two modal unbalances are expressed as:

$$U_{c1}\,\psi_{1,b1} + U_{c2}\,\psi_{1,b2} = -\bar{U}_1 \qquad (5.1)$$

$$U_{c1}\,\psi_{2,b1} + U_{c2}\,\psi_{2,b2} = -\bar{U}_2 \qquad (5.2)$$

where

$U_{c1} = Uc1 \quad \phi_{c1}$: correction mass imbalance at balance plane 1

$U_{c2} = U_{c2} \quad \phi_{c2}$: correction mass imbalance at balance plane 2

$\psi_{1,b1} \quad \psi_{1,b2}$: first mode shape components at the two balance planes

$\psi_{2,b1} \quad \psi_{2,b2}$: second mode shape components at the two balance planes

$\bar{U}_1, \bar{U}_2$: first and second modal unbalances calculated as described in section 3

Equations 5.1 and 5.2 may then be solved for the correction weights and these attached to the shaft as shown in Figure 9.

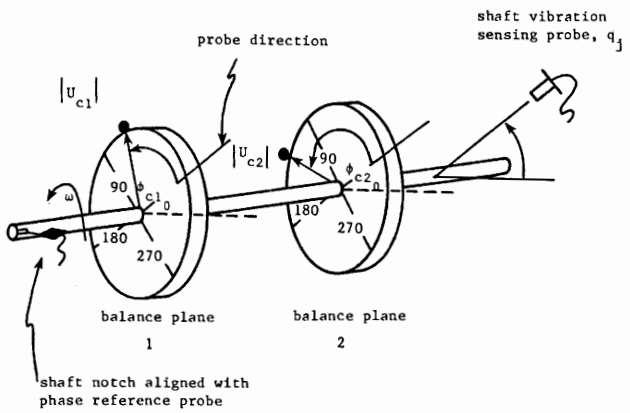

Fig. 9. Diagram for the attachment of the two correction imbalances required for the elimination of two modal unbalances.

The mathematical representation of a rotor bearing system presented has some limitations. These arise mainly from the assumptions of symmetry and proportional damping used in the analysis. Hence, the methods presented may be more effective in certain classes of machinery than in others. Those most likely to exhibit response characteristics in agreement with the theory will have rotors supported in anti-friction or tilting pad journal bearings. These elements are generally known to possess very small asymmetric cross-coupling forces. The machines which may respond in a fashion differing from the theory are those (1) with rotors supported in sleeve-type journal bearings (Reference 10), (2) with overhung wheels producing gyroscopic forces (Reference 11), (3) and rotors with considerable seal related dynamic forces (Reference 12). These configurations are known to produce asymmetric cross coupling forces between the shaft's two geometric radial planes.

CONCLUSIONS

A technique has been theoretically and experimentally developed to approximate the effective unbalances in a rotor. This has generally been accomplished by analytically developing the relationship between the rotor's unbalance response and its inherent unbalance distribution. The graphical procedure developed to separate the critical speed from the unbalance response peak provides for a more accurate evaluation of the effective unbalance. This method can be used in conjunction with influence coefficient balancing to judiciously choose proper trial weights.

A practical application was presented on the steam turbine driver of a hydrogen gas compression train. This example illustrates the experimental data and procedure required to implement the balancing technique. Finally, the method is shown to be applicable to higher mode balancing.

There are several limitations to this procedure that should be noted. The rotor must be capable of operating through the critical speed region, and also the rotor system should be lightly damped. In the case of heavily damped rotors, an additional correction factor must be incorporated which relates the difference in phase angle observed at the probe position as compared to the rotor phase angle at the center span.

ACKNOWLEDGEMENTS

The authors would like to express their appreciation for the assistance provided by the late Professor Henry Black, Heriot Watt University, United Kingdom and Mr. Donald Bently, Bently Nevada Company, whose suggestions and insight were of great help in the paper's development.

REFERENCES

1. Parkinson, A. G., Jackson, K. L., Bishop, R. E. D., "Some Experiments on the Balancing of Small Flexible Rotors: Part I - Theory, Part II - Experiments," Journal Mechanical Engineering Science, Volume 5, 1963.

2. Lindley, A. L. G., Bishop, R. E. D., "Some Recent Research on the Balancing of Large Flexible Rotors," Proceedings of the Institute of Mechanical Engineers, Volume 177, No. 30, 1963.

3. Bishop, R. E. D., Parkinson, A. G., "On the Use of Balancing Machines for Flexible Rotors," Trans. ASME, Journal of Engineering for Industry, May, 1972.

4. Bishop, R. E. D., Parkinson, A. G., "Vibration and Balancing of Flexible Shafts," Applied Mechanics Review, Volume 21, No. 5, May, 1968.

5. Parkinson, A. G., Bishop, R. E. D., "Vibration and Balancing of Rotating Continuous Shafts," Journal Mechanical Engineering Science, Volume 3, No. 3, 1961.

6. Kellenberger, W., "Balancing Flexible Rotors on Two Generally Flexible Bearings," The Brown Boveri Review, Volume 54, September, 1967.

7. Lindsey, J. R., "Significant Developments in Methods for Balancing High Speed Rotors," Trans. ASME, 69-VIBR-53.

8. LeGrow, J. V., "Multiplane Balancing of Flexible Rotors - A Method of Calculating Correction Weights," Trans. ASME, 71-VIBR-52.

9. Bently Nevada Corporation, "Orbits," Minden, Nevada, 1970.

10. Black, H. F., Nutall, S. M., "Modal Resolution and Balancing of Synchronous Vibrations in Flexible Rotors with Non-Conservative Cross Coupling," Institute of Mechanical Engineers, C182/76, 1976.

11. Green, R. B., "Gyroscopic Effects on the Criticcal Speeds of Flexible Rotors," Trans. ASME, Journal of Applied Mechanics, December, 1948.

12. Black. H. F., "Effects of Hydraulic Forces in Annular Pressure Seals on the Vibrations of Centrifugal Pump Rotors," Journal Mechanical Engineering Science, Volume 11, No. 2, 1969.

13. Klosterman, A. L., "On the Experimental Determination and Use of Modal Representations of Dynamic Characteristics," Doctoral Dissertation, University of Cincinnati, 1971.

14. Clough, R. W., Penzien, J., "Dynamics of Structures," McGraw-Hill, 1975.

15. Choy, K. C., Gunter E. J., and P. E. Allaire, "Fast Fourier Transform Analysis of Rotor-Bearing Systesm," ASME "Topics in Fluid Film Bearing and Rotor Bearing System Design and Optimization," April 1978.

APPENDIX A

The dynamical equations of motion of a multimass rotor-bearing system may be expressed in terms of discrete mass, damping, and stiffness matrices as follows (15)

$$[M]\{\ddot{q}\} + [C]\{\dot{q}\} + [K]\{q\} = \{F(t)\} \qquad (A.1)$$

Assuming zero damping and no forcing functions acting on the system, the standard eigenvalue problem is as follows

$$\{-\omega_r^2[M] + [K]\}\{\psi_r\} = \{0\} \qquad (A.2)$$

The function ψ^r is a planar mode shape of the system corresponding to the rth mode (rth eigenvector). These mode shapes may also be generated by a standard critical speed program using matrix transfer theory. In this case the mode shapes are normalized displacement (and rotation mode shapes) rather than orthonormal modes. Assuming symmetric mass and stiffness matrices, the mode shapes satisfy the standard orthogonality conditions (13,14)

$$\{\psi_r\}^T [M]\{\psi_s\} = \begin{cases} 0 & , \quad r \neq s \\ m_r & , \quad r = s \end{cases} \qquad (A.3)$$

$$\{\psi_r\}^T [K]\{\psi_s\} = \begin{cases} 0 & , \quad r \neq s \\ k_r & , \quad r = s \end{cases} \qquad (A.4)$$

The quantites m_r and k_r are referred to as the modal mass and modal stiffness of the system, respectively. Note that by premultiplying equation A.2 by $\{\psi_r\}^T$ and using (A.3) and (A.4) shows

$$\omega_r^2 = \frac{k_r}{m_r} \tag{A.5}$$

The response vector $\{q\}$ of the system may be expressed in terms of the sum of the generalized modal coordinates γ_r and mode shapes ψ_r as follows

$$\{q\} = \sum_{s=1}^{n} \gamma_s \{\psi_s\} \tag{A.6}$$

where

n: total number of modal degrees of freedom

γ_s: sth mode shape coefficient.

Premultiplying equation A.1 by $\{\psi_r\}^T$ and substituting equation (A.6) yields

$$\{\psi^r\}^T [M] \sum_{s=1}^{n} \ddot{\gamma}_s \{\psi_s\} + \{\psi_r\}^T [C] \sum_{s=1}^{n} \dot{\gamma}_s \{\psi_s\}$$

$$+ \{\psi_r\}^T [K] \sum_{s=1}^{n} \gamma_s \{\psi_s\} = \{\psi_r\}^T \{F(t)\} \tag{A.7}$$

Applying the orthogonality conditions A.3 and A.4 in A.7 shows

$$m_r \ddot{\gamma}_r + C_{rs} \dot{\gamma}_s + k_r \gamma_r = \{\psi_r\}^T \{F(t)\} \tag{A.8}$$

where $C_{rs} = \{\psi_r\}^T [C] \{\psi_s\}$

In most structural vibration problems, where the modal damping is only several percent of critical damping, the damping matrix is assumed to be a "proportional" damping matrix. Reference 14 demonstrates that the general form of the damping matrix required to satisfy this property is

$$[C] = [M] \sum_i a_i \{[M]^{-1} [K]\}^i \tag{A.9}$$

where

$$i \in \{0, \pm 1, \pm 2, \ldots\}$$

and a_i are arbitrary constants.

In this event the damping matrix satisfies a similar orthogonality condition as the mass and stiffness matrices,

$$\{\psi_r\}^T [C] \{\psi_s\} = \begin{cases} 0 & , \quad r \neq s \\ c_r & , \quad r = s \end{cases} \tag{A.10}$$

Assuming proportional damping equation (A.8) becomes

$$m_r \ddot{\gamma}_r + c_r \dot{\gamma}_r + k_r \gamma_r = \{\psi_r\}^T \{F(t)\} \tag{A.11}$$

For the case of a multi-mass flexible rotor in fluid film bearings, the damping on the shaft is acting at discrete locations. Under these circumstances, the use of the planar modes as a set of orthogonal functions, will not completely uncouple the modal equations of motion. This is because the damping matrix is, in general, not proportional to either the mass or the stiffness matrix.

Consider as an example a multistage compressor with the following characteristics and modal displacement coordinate at the bearings.

Table A.1

Rotor Modal Characteristics

Mode	Modal Weight W_l	Critical Speed N_c	BRG Damping C_{xx}	BRG Modal Displacement ψ_{i1}	ψ_{i2}	Modal Damping Matrix C_{11}	C_{12}	C_{13}
1	600	4500	1200	.2	.2	96	0	432
2	400	9800	1200	-.8	.8	0	1536	0
3	800	21,000	1200	.9	.9	432	0	1944

Table A.1 shows that for the particular case of a symmetric turborotor, the first and second modes are uncoupled because the cross-coupled modal damping coefficient between the first and second modes is zero. However, such is not the case with the third mode. Note that there is a sizable third mode cross coupling coefficient C_{13} associated with the first planar modal equation which must be taken into consideration. The implication of this higher modal coupling through the damping matrix is that the motion of the rotor cannot be expressed as a planar function of only the first mode shape. The discrete damping at the bearing causes the mode shape to warp out of the plane of the undamped mode. This warping effect is more pronounced as one observes the motion closer to the bearing and must be accounted for when performing modal balancing by means of proximity probe measurements near the bearing.

Assume that the forcing function $\{F(t)\}$ acting on the rotor system is caused by an arbitrary distribution of unbalance $\{U\}$ along the shaft. The synchronous forcing function may be expressed in complex form as

$$\{F(t)\} = \omega^2 \{U\} e^{i\omega t} \tag{A.12}$$

Dividing by the modal mass m_r, the modal equations of motion are given by

$$\ddot{\gamma}_r + 2\omega_r \xi_{rs} \dot{\gamma}_s + \omega_r^2 \gamma_r = \omega^2 E_r e^{i\omega t} \tag{A.13a}$$

where

$$\xi_{rs} = \frac{\{\psi_r\}^T [C] \{\psi_s\}}{2 m_r \omega_r}$$

E_r = modal unbalance eccentricity

$$= \frac{\{\psi_r\}^T \{U\}}{m_r} = \Lambda_r + i\mu_r \tag{A.13b}$$

Assuming synchronous shaft motion, let $\gamma_r(t) = \gamma_r e^{i\omega t}$. Equation (A.8) reduces to

$$(\omega_r^2 - \omega^2 + 2i\omega\omega_r \xi_{rr}) \gamma_r + i2\omega_r \omega \xi_{rs} \gamma_s = \omega^2 E_r \tag{A.14}$$

The modal steady state equation of motion may be put in dimensionless form by dividing by the ω_r^2 as follows

$$(1 - f_r^2 + i2\,\xi_{rr} f_r)\gamma_r + i2\, f_r\, \xi_{rs}\, \gamma_s = f_r^2\, E_r \quad (A.15)$$

Table A.2

Rotor Dim Modal Damping Coef. And Amplification Factors

Mode	ω_r rad/sec	C_r critical damping	ξ_{r1}	ξ_{r2}	ξ_{r3}	A_{cr}	A_{ur}
1	471	1465	.064	0	0.295	7.81	7.83
2	1026	2126	0	0.722	0	.693	1.000
3	2200	3419	0.126	0	0.5886	.85	1.05

The natural frequencies and modal damping coefficients for a typical multi-stage compressor with two damped resonance frequencies in the operating range, are given in Table A.2. The value of A_{cr} represents the amplification factor at the undamped critical speed and the value of A_{ur} represents the maximum modal amplification factor. Note that, although the second critical speed is within the compressor operating speed range, it is critically damped ($A_u = 1$). The first mode will have a substantial amplification factor at the first critical speed. Table A.2 also shows that the modal cross coupling coefficient ξ_{13} is over 4 times larger than the principal first modal damping coefficient ξ_{11} and hence cannot be arbitrarily dropped from the analysis.

Assume that the turborotor is operating near the first critical speed such that $f_1 = 1$, $f_2 = 0.46$ and $f_3 = 0.21$. The governing equations for the magnitude of the modal coordinates γ_r is given by A.15 and reduces to

$$(1 - f_1^2 + i\ .128\ f_1)\gamma_1 + i\ 0.590\ f_1\ \gamma_3 = f_1^2\ E_1$$

$$(.7884 + i\ .6642)\ \gamma_2 = .2116\ E_2$$

$$(.956 + i\ .2472)\gamma_3 + i\ .0529\ \gamma_1 = .04\ E_3 \quad (A.16)$$

The simultaneous solution of the above complex algebraic equations yields the values of the modal coefficients in terms of the modal unbalance eccentricities E_1, E_3. However, when operating near the first critical speed only about 4% of the third modal unbalance eccentricity E_3 is excited. One could then approximate the modal coefficient γ_3 by

$$\gamma_3 = -\frac{i\ 2\ \xi_{31}\ f_3\ \gamma_1}{(1 - f_3^2 + 2\ i\ \xi_{33}\ f_3)} \simeq - i2\xi_{31} f_3 \gamma_1 \quad (A.17)$$

The total rotor motion is given by

$$\{q\} = \gamma_1\ \{\psi_1\} + \gamma_2\ \{\psi_2\} + \gamma_3\ \{\psi_3\} \quad (A.18)$$

Ignoring the contribution of the second mode for the time being, the rotor motion operating near the first critical speed is given by

$$\{q\} = \gamma_1\ [\{\psi_1\} - 2\ i\ \xi_{31}\ f_3\ \{\psi_3\}] \quad (A.19)$$

This shows that the displacement of the rotor near the first critical speed is composed of the first planar mode $\{\psi_1\}$ with the addition of approximately 5% of the third mode which lags about 90° behind. This addition of the third mode component with a phase lag is what accounts for the skewed shape of the space curve of the rotor centerline. Thus we see that the rotor is not perfectly planar due to the action of bearing damping at the ends of the shaft. This skewed effect becomes more pronounced as we measure the rotor motion closer to the bearing ends. If the monitoring probes are placed at least one-quarter span inboard from the bearing locations, then shaft skew due to the third mode excitation does not have to be taken into consideration in the balancing procedure.

Note also if Equation (A.17) is substituted into Equation (A.16) then we obtain

$$(1.03 - f_1^2 + i\ 2\ \xi_{11}\ f_1)\ \gamma_1 = f_1^2\ E_1 \quad (A.20)$$

This equation implies that the first natural frequency appears to increase by 1.5% due to the influence of the third mode.

In the particular example cited, it was seen that the second mode was critically damped. In practice it has been found that for the normal turborotor design with the impeller discs located between the bearings, the second critical speed amplification factor is normally much lower than the first critical speed amplification factor. Therefore if displacement measurements are taken reasonably close to the rotor center span, the first modal equation of motion is a reasonable approximation of the shaft behavior. The small contribution due to the second mode is minimized since the shaft center span is a node point.

Neglecting modal coordinate cross coupling, the rotor response vector is given by

$$\{q\} = e^{i\omega t} \omega^2 \sum_{r=1}^{n} \frac{\{\psi^r\}^T\{U\}}{m_r\ (-\omega^2 + i2\omega\ \omega_r\ \xi_r + \omega_r^2)}\ \{\psi^r\} \quad (A.21)$$

The complex displacement coefficient, i.e. amplitude and phase angle, for any particular degree of freedom is given by

$$q_j = \sum_{r=1}^{n} \frac{(\Lambda_r + i\mu_r)\ f_r^2\ \psi_{rj}}{(1 - f_r^2 + i2\ \xi_r\ f_r)} = \Sigma\ E_r\ A_r\ \psi_{rj} \quad (A.22)$$

where A_r = frequency dependent modal amplification factor for rth mode

$$= \frac{f_r^2}{1 - f_r^2 + i2\ \xi_r\ f_r}$$